

POURING AND SOLIDIFICATION OF A METAL INGOT

C.W. Hirt and R.P. Harper  
December 24, 1988

OBJECTIVE

---

A previous Technical Note, "FLOW-3D Solidification/Melting Update," (FSI-88-TN14) described an addition to the 1988 version of the FLOW-3D computer program. This addition improved the modeling of liquid/solid phase changes by allowing for a latent heat of fusion and for differing physical properties in the two phases. The model was illustrated and verified through comparison with experimental data involving a confined flow situation.

In this note we further illustrate the new capability with a combined free-surface flow and heat transfer problem associated with the production of an aluminum ingot. No experimental data is publically available for the problem treated here, but the geometry and physical parameters have been chosen to be representative of a realistic situation.

Three calculations are presented in the following sections, which differ only in the specification of which boundaries are allowed to conduct heat. A comparison of the three results shows that fluid-dynamic and heat-transfer processes are quite strongly coupled in this example.

In the next section the specific casting problem treated in this note is described in detail. The remaining sections contain a description of the three calculations and a summary of the findings. All calculations reported here were performed with the extended 1988 version of FLOW-3D as described in Technical Note 14.

THE INGOT PROBLEM

---

A basic operation in any foundry is the casting of ingots. These prismatic shapes are usually formed by the pouring of molten metal into a mold. In this note we consider the pouring and solidification of pure aluminum ingots. For simplicity in demonstrating the type of information to be gained from a FLOW-3D

simulation we have restricted the problem to two-dimensions. Three-dimensional computations could be performed by FLOW-3D in a similar fashion (of course, the computational effort would be significantly larger).

In the present case the pouring region is located at the center of the mold and the flow is presumed to spread symmetrically left and right. Only the right symmetric half of the problem needs to be modeled. The right half of the mold is 30.0 cm wide and 10.0 cm high, however, there is a two centimeter outlet at the top of the right wall so that the mold can only be filled to a maximum depth of 8.0 cm.

The inlet flow enters the right half mold at the top left corner by flowing down a vertical channel 1.0 cm wide. At the bottom of this channel is an arrangement of baffles and screens designed to keep the flow from splashing and helping it to more uniformly fill the mold. Figure 1 shows the geometric setup for the symmetric right half except for the outlet hole. The screens, which complete the boxlike baffle, have a porosity of 0.95 and exert a flow loss on the metal proportional to the square of the flow velocity. The screen loss coefficient is 0.2.

The inlet flow velocity is specified to be a constant 30.0 cm/s, however, the liquid metal flow is only allowed to enter the system with this velocity during the first 7.9 s and then is linearly ramped to zero by 8.1 s. If no metal flows out the outlet, the net flow in is just enough to fill the mold to its maximum level. It is further assumed that the incoming flow has a constant temperature of 760° C.

Physical parameters for the aluminum were taken to be those shown in the following table in CGS units:

Density . . . . .	2.7 g/cc
Liquid specific heat . . . . .	8.37E+6 erg/g/K
Solid specific heat . . . . .	9.21E+6 erg/g/K
Liquid thermal conductivity . . . . .	1.88E+7 erg/s/cm/K
Solid thermal conductivity . . . . .	2.09E+7 erg/s/cm/K
Latent heat . . . . .	3.94E+9 erg/g
Fusion temperature . . . . .	660° C
Thermal expansion coefficient . . . . .	3.0E-5 1/K
Reference temperature . . . . .	660° C

Because the metal is assumed to be pure aluminum, no mushy zone is modeled (i.e., liquidus and solidus temperatures are equal to the temperature of fusion).

In the first calculation all heat transfer effects were ignored, corresponding to a completely insulated mold. In the second case the bottom of the mold was set at a constant temperature of 50° C and the heat transfer coefficient at this boundary was 2.09E+6. This value is about nine times smaller than pure conduction to account for less than perfect wetting of the surface of the mold and for possible entrapment of gas along the boundary. Finally, the last case simulated included heat transfer not only at the bottom but also at the right side wall. The heat transfer coefficient at the right wall was taken to be twice that at the bottom wall and the right wall temperature was held constant at 30° C. No radiation or conduction was allowed at the free surface of the metal.

#### THE COMPUTATIONAL MODEL

---

For this problem a uniformly zoned mesh was selected that contained 30 cells horizontally and 10 cells vertically. All cells are square with edge length of 1.0 cm, as shown in Fig. 2. Since the inlet channel is only one mesh cell wide, this numerical resolution is rather coarse but deemed acceptable for the gross filling and solidification characteristics.

To define the basic free-surface flow problem in Namelist XPUT we set ITB=1 and gravity GZ=-980.0 cm/s/s. The default setup assumes incompressible flow and no fluid initially in the mesh, which are the desired conditions. Boundary conditions were set to have rigid walls at the bottom, right and top sides of the mesh, while the left, front and back sides were treated as planes of symmetry. The top boundary was defined to be a specified inflow boundary with the necessary time dependence to ramp the inflow to zero between 7.9 and 8.1 s. The inflow temperature was set at 760° C. To define the outflow at the right side wall this boundary was specified as a constant pressure boundary with a zero (gage) pressure.

In order to limit the inflow and outflow regions along the top and side walls, respectively, it is necessary to define obstacles blocking those portions of these boundaries where flow is not to occur. In addition, in the third problem to have heat transfer at the right side wall it must be remembered that the obstacle (obstacle number 2 in the file shown in Fig. 3) is really the side wall boundary for which one must specify the temperature and heat transfer coefficient.

Recognizing the limited resolution and possible splashing of metal at early times it was concluded that the defoaming option, IFPK=2, would be useful in this problem. (See Technical Note FSI-88-TN10 for a discussion of this option.) Using the inlet velocity as a typical velocity for the problem the time-step size was initially set at 0.01 s and the SOR pressure iteration convergence criterion was set to be 0.005.

A complete listing of the input file for the third problem, which contained the maximum number of heat transfer surfaces, is given in Fig. 3. Input for the first two problems can be easily generated from this file by selectively turning off the options not wanted. For example, for the second problem it is only necessary to omit the temperature and heat transfer coefficient associated with the second obstacle in Namelist OBS. For the first problem, which has no heat transfer at all, one must turn off this feature by resetting in Namelist XPUT the parameters IFENRG=0, IFRHO=0, IMPHTC=0, IHTC=0 and TL1=TS1=0.0.

## COMPUTATIONAL RESULTS

---

Some organization is needed to summarize the considerable output of the three calculations. With this in mind we first review the results of the third, and most realistic, case that is cooled through both the bottom and the right side walls. Then some comparisons will be made between this case and the other cases subjected to less severe cooling rates. These comparisons will show how changing the cooling surfaces can dramatically change the solidification history of the ingot.

### Maximum-cooled Case

Heat transfer is not particularly important during the first few seconds of pouring, except possibly for the formation of thin sheets of metal that splash up on the cooled walls. (Such fine scale detail cannot be represented in the present coarse mesh model.) Figure 4 shows the flow computed during the first three seconds following the initiation of the pour. To make these plots a modification was necessary to the plot request file. FLOW-3D usually plots velocities only in those mesh cells that are more than half full of fluid. For the data shown in Fig. 4 this prescription would result in only a few cells being plotted because at early times the coarse mesh does not contain many cells that are more than half full of fluid. In particular, the stream of fluid leaving the baffle box and falling to the floor of the mold would not be visible. For Fig. 4, then, we reduced the cutoff value of 0.5 for the fraction of fluid to 1.0E-6,

which insures that all cells containing fluid are plotted.

According to the results shown in Fig. 4 the incoming flow is strongly deflected toward the right wall, which it reaches in less than one second. A splash occurs in the lower right corner that sends some fluid to the top right corner. A small amount is trapped at the top corner for some time before eventually leaving the mesh through the outflow port. Fluid continues to pile up at the right sending a hydraulic jump moving back to the left. By three seconds this leftward-moving flow has reached the left boundary of the mold. The lowest temperature in the mesh at  $t=3.0$  s is  $682^{\circ}$  C, and is located at the free surface adjacent to the cold right wall.

Following the initial transients, the coldest region in the mesh is the lower right corner because it is losing heat through both the side and bottom walls. Figure 5 shows the temperature history of the corner mesh cell in this region. The maximum temperature never quite reaches the  $760^{\circ}$  C inflow value presumably because of cooling as the fluid traverses the lower boundary. At approximately 4 s the fluid in this cell reaches its fusion temperature of  $660^{\circ}$  C and solidifies. The cell remains at  $660^{\circ}$  C while its latent heat is removed. This takes approximately 3 seconds, and then the temperature monotonically subcools during the remainder of the computation.

The subsequent flow and temperature distribution at selected times up to 30.0 s are shown in Figs. 6-7. In Fig. 6 it can be seen that the inflow has stopped between the top plot at  $t=6.02$  s and the middle plot at  $t=9.04$  s. It will also be noted that in the last plot at  $t=12.1$  s there are trapped bubbles along the right wall. These bubbles form because the fluid in these mesh cells reached the solidification temperature before the cells had time to completely fill. This is partly a fault of the model, which has limited resolution and does not distinguish separate phase velocities within a cell. It may also indicate that the rapid cooling in this region, coupled with the presence of a free surface, could lead to some air entrapment and/or shrinkage bubbles.

During the time shown in Fig. 6 the free surface has settled to a nearly flat surface with only low amplitude surface waves. At the bottom of the mold the metal has solidified near the lower right corner by  $t=6.02$  s, but by  $t=12.06$  s it has solidified over the entire bottom as well as the two right-most columns of cells.

In the late time plots of Fig. 7 the dominance of natural convection is clearly evident at the solidification front moving in from the right side. The solidification of the second row of cells up from the bottom is also evident in these plots. (To

properly compare these plots it is necessary to note that the velocity vector lengths are rescaled in each plot. The maximum velocity in each plot is recorded at the top left corner of the plot frame.)

### Influence of Cooling Boundaries

A comparison of the computed flow with no cooling versus that with cooling through one or two walls is shown in Fig. 8 at a problem time of  $t=9.0$  s. The walls supporting heat transfer have been marked by cross hatching. In the no-heat-transfer case (top plot) the large eddy flow is a residual of the filling process. The case with bottom heat transfer only (middle plot) exhibits some solidification along the bottom, which has significantly changed the flow structure. In the maximum-heat-transfer case (bottom plot) the entire bottom layer of metal has solidified and the flow is changing to a natural convection dominated flow. Reference to the temperature contours also shows that at this time only the maximum-cooled case has regions of subcooled metal.

At later times, say at  $t=24.1$  s as shown in Fig. 9, the bottom-cooled case has its hottest metal at the free surface adjacent to the right wall, while in the maximum-cooled case it is closer to the center of the mold. (No example of the uncooled case is shown here because it was only carried out to a time of 10.0 s.)

Although both cases shown in Fig. 9 have clockwise rotating eddy structures, these eddies develop in different ways. By reviewing intermediate time plots one learns that in the bottom-cooled case the eddy is a residual of the pouring process. As time progresses, this eddy drifts to the right and weakens. It is this eddy that moves the maximum temperature location to the insulated right wall. In contrast, in the maximum-cooled example the eddy generated by pouring is destroyed by solidification and natural convection effects; but at later times natural convection, driven by side wall cooling, reestablishes a clockwise eddy. Close inspection of the plots in Fig. 9 reveals that the structure of the two eddies is, in fact, different. In the bottom-cooled case the eddy is broad with several cells defining downward flow on its right side, while in the maximum-cooled case the eddy is much more concentrated near the solidification front.

In all cases the recirculating eddy flow generated by the pouring through the baffle box helps to keep the temperature relatively uniform in the upper central region of the mold. The temperature is most uniform in the maximum-cooled case because of the greater influence of natural convection, which suggests that fewer problems from solidification shrinkage or stress are likely to occur in this case.

## SUMMARY

---

These results have shown how FLOW-3D can be used to investigate a simple casting problem. Although the geometry is not particularly complicated, the flow and heat transfer processes are nontrivial and much remains to be learned from this type of analysis. For example, it would be useful to study the effects of variations in the baffle arrangement, different pouring rates and pouring temperatures, and different wall temperatures.

In this paper the principal effort was to compare different arrangements of cooling surfaces in the mold. The comparison of Three calculations has shown how insulating different boundaries of the mold can significantly change the solidification history of the ingot.

The calculations reported in this note did not require excessively long computational times. For the case with no heat transfer, for example, the CPU time to reach a problem time of 10.0 s was 3.97 hours on a MicroVAX II computer. With heat transfer the CPU time increases to 4.10 hours to reach the same problem time. To reach a problem time of 25.0 s the two heat transfer cases each required a total CPU time of 6.99 hours. Note that less CPU time is needed to advance the solution at later times. At early times a small time-step size must be used because of large velocities generated during the initial filling and splashing period. As time progresses, the time-step size increases and more problem time is modeled in fewer time cycles (i.e., in less CPU time).

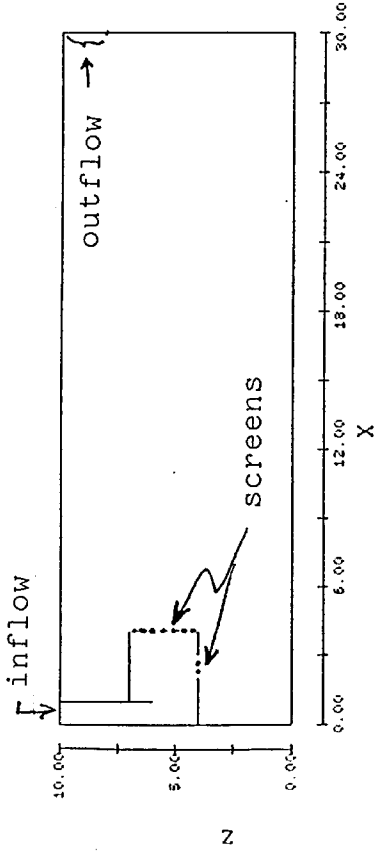


Fig. 1. Geometric setup for symmetric right half of mold.

X-Z MESH

NUMBER OF CELLS= 30  
 X 10  
 Z 10  
 SMALLEST CELL= 1.000E-00  
 LARGEST CELL= 1.000E-00  
 MAXIMUM CELL RATIO= 1.000E+00  
 AT CELL 30

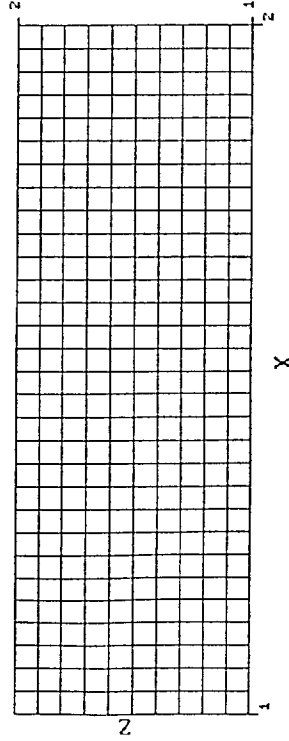


Fig. 2. Mesh used in all calculations (30 x 10 cells).

```

AL CAST + HEAT
$XPUT
IFPK=2,
IHD=1,
IHTC=1,
WR=5,
WBCT(2,6)=-30.,
FBCT(1,2)=0.0,
TIMBCT(2)=8.1,
TBCT(1,5)=50.,
TBCT(2,2)=760.,
RWALL(1)=0.0,
RWALL(4)=0.0,
THXF1=3.0E-5,
TSL=660.0,
THCS1=2.09E+7,
HWALL(5)=2.09E+6,
DELT=0.01,
PRDTR=100.,
$END
$MESH
NXCELT=30,
NYCELT=1,
NZCELT=10,
$END
$SOBS
NOBS=2,
CZ(1)=-1.0,
CZ(2)=-1.0,
HOB(1,2)=4.186E+6,
$END
$SFL
$END
$SFB
NBAFS=6,
BCX(1)=1.0,
BCZ(2)=1.0,
BXH(2)=4.0,
BCZ(3)=1.0,
BCZ(4)=1.0,
BXH(4)=4.0,
BCZ(5)=1.0,
BXH(5)=3.0,
BCX(6)=1.0,
BZH(6)=7.0,
$END
$TEMP
$END
$MOTN
$END
$GRAFIC
NVPLTS=1,
NCPLTS=3,
ILOCC(1)=31,
$END
$PARTS
$END
IMPHTC=1,
IFENRG=2,
GZ=-980.,
WT=6,
WBCT(1,6)=-30.,
FBCT(2,6)=0.0,
TIMBCT(1)=7.9,
TBCT(2,6)=760.,
TBCT(1,2)=760.,
RWALL(3)=0.0,
RHOF=2.7,
TL1=660.0,
THC1=1.88E+7,
CVSI=9.21E+6,
PLTDT=1.0,
IFRHO=1,
WB=2,
WBCT(1,6)=-30.,
FBCT(2,6)=0.0,
TIMBCT(1)=7.9,
TBCT(2,6)=760.,
TBCT(1,2)=760.,
RWALL(3)=0.0,
RHOF=2.7,
TL1=660.0,
THC1=1.88E+7,
CVSI=9.21E+6,
PLTDT=1.0,
PX(2)=30.,
PY(2)=1.0,
PZ(2)=10.,
CC(1)=9.99,
CC(2)=29.99,
TWOBS(1,2)=30.0,
XL(1)=1.0,
ZH(2)=8.0,
BZL(1)=6.0,
BXL(2)=1.0,
BXH(3)=2.0,
BXL(4)=3.0,
BXL(5)=2.0,
KBAF2(5)=0.2,
BZL(6)=4.0,
KBAF2(6)=0.2,
KONTYP(1)=5,
JLOCC(1)=2,
KONTYP(2)=7,
KLOCC(1)=2,

```

Fig. 3. Namelist input file for maximum cooled case. All units are CGS.

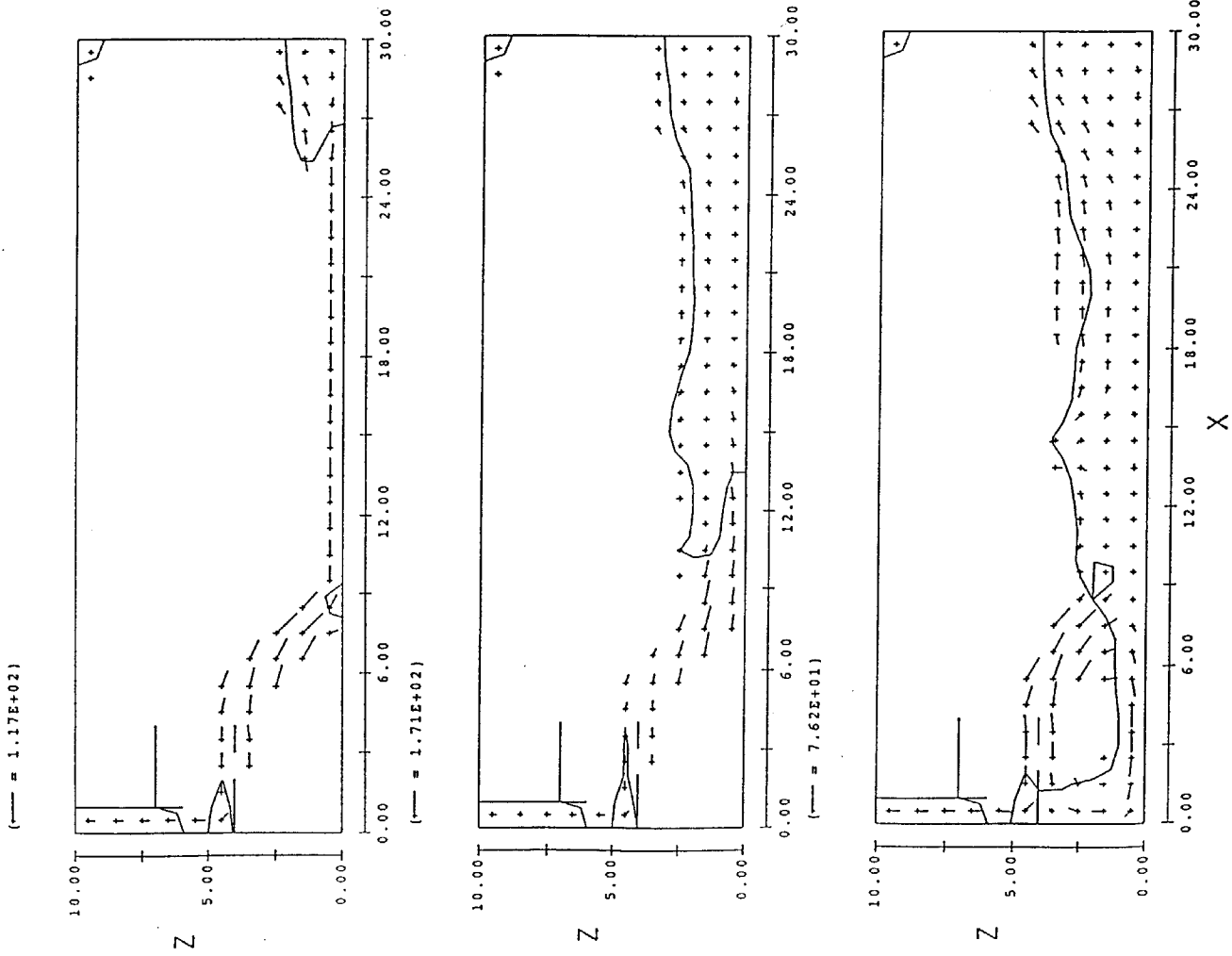


Fig. 4. Computed flow at early times: 1.0 s top, 2.0 s middle and 3.0 s bottom.

AT CELL (31, 2, 2)

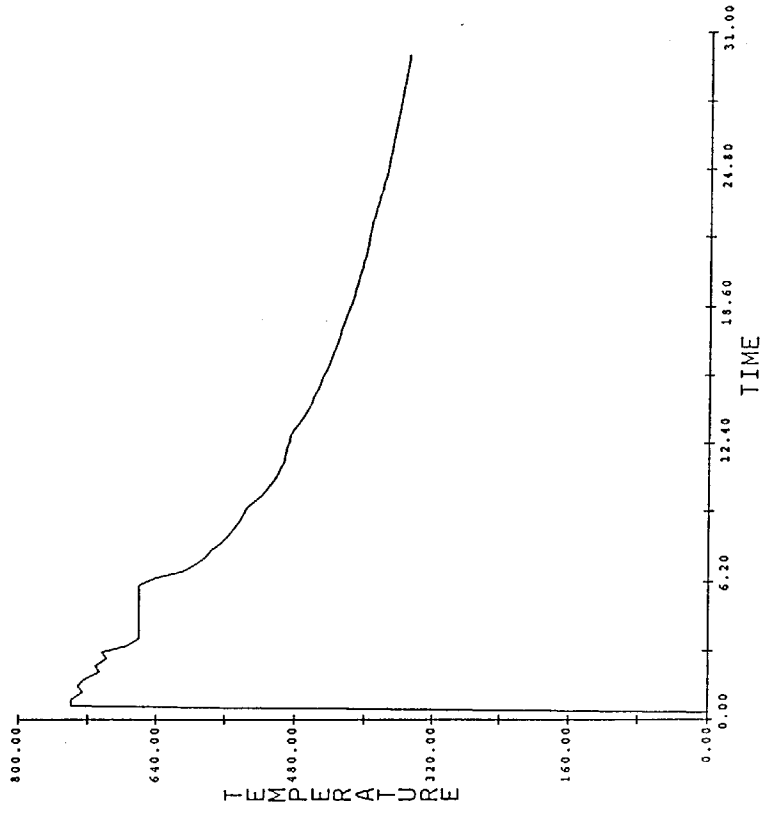
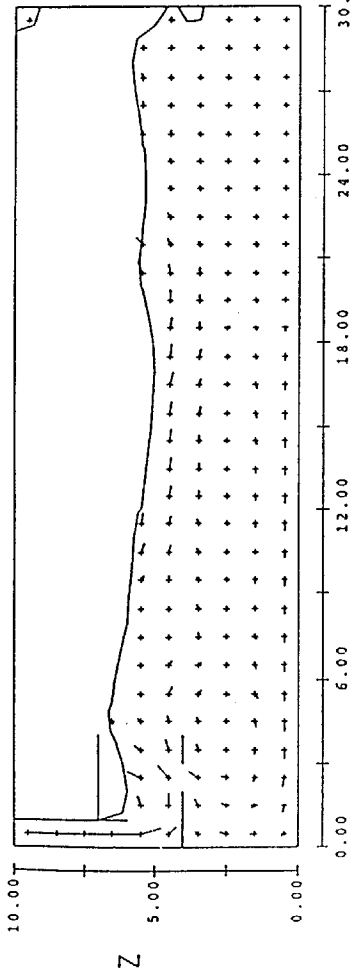
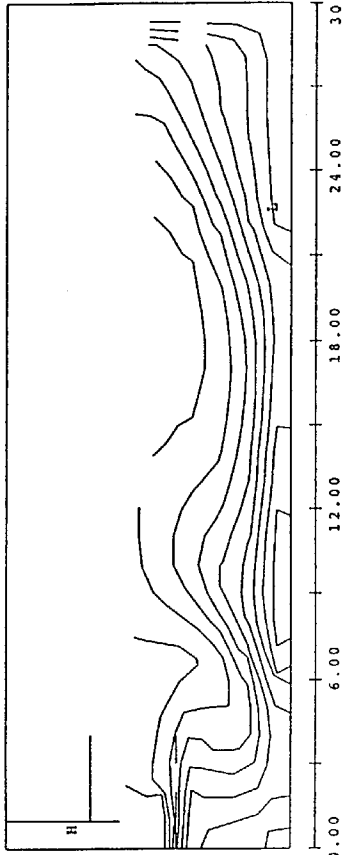


Fig. 5. Temperature history of mesh cell in lower right corner. Temperature in degrees Centigrade. Plateau is at fusion temperature of 660°C.

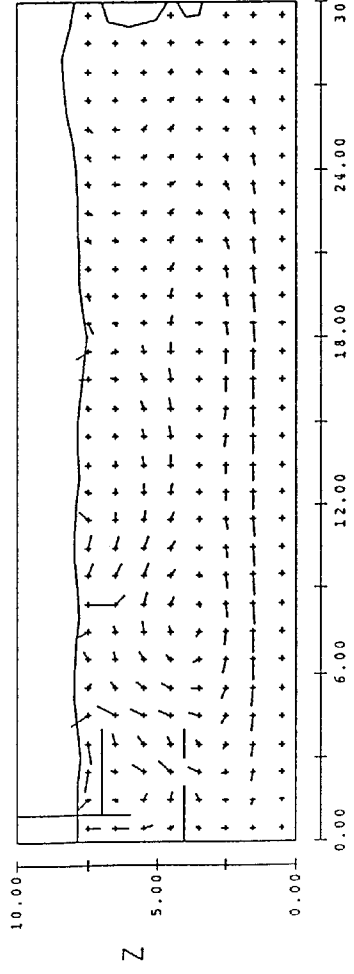
(--- = 3.00E+01)



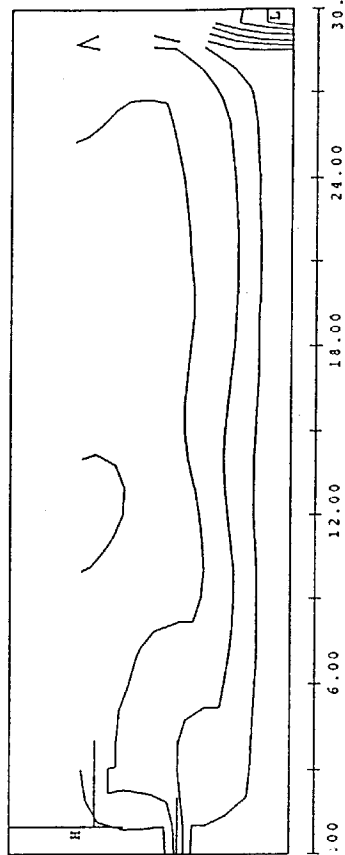
(LOW= 6.600E+02 LOW CONTOUR= 6.650E+02)  
(HIGH= 7.600E+02 HIGH CONTOUR= 7.550E+02)



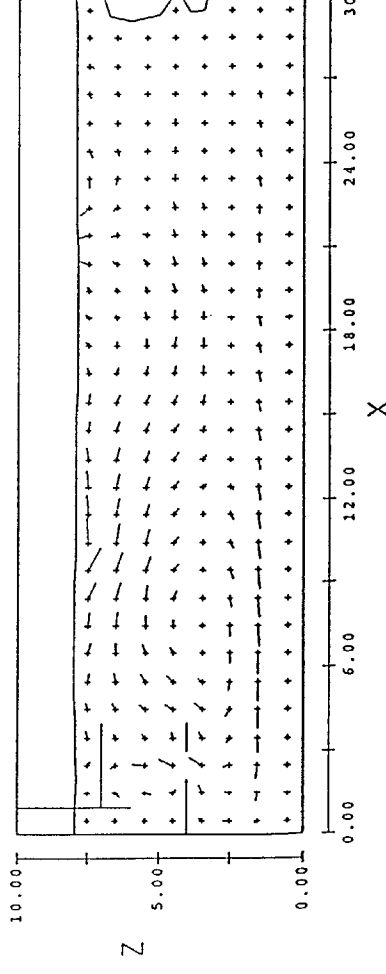
(--- = 1.09E+01)



(LOW= 5.419E+02 LOW CONTOUR= 5.526E+02)  
(HIGH= 7.551E+02 HIGH CONTOUR= 7.444E+02)



(--- = 5.69E+00)



(LOW= 4.895E+02 LOW CONTOUR= 5.019E+02)  
(HIGH= 7.367E+02 HIGH CONTOUR= 7.243E+02)

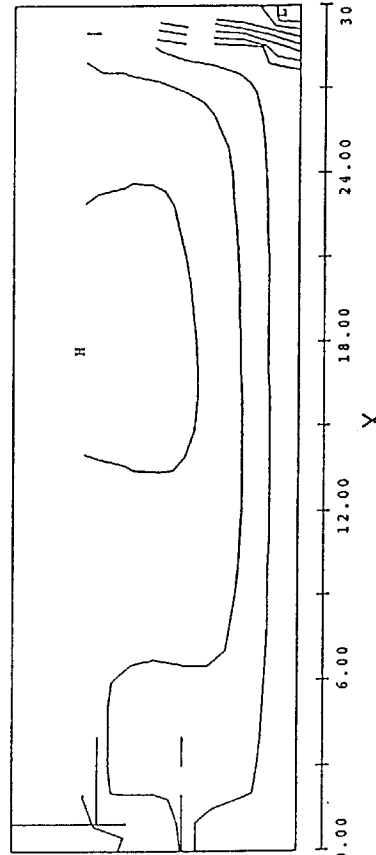


Fig. 6. Flow Configuration and temperature contours for maximum cooled case: 6.0 s top, 9.0 s middle and 12.1 s bottom.

